

Highly effective and reproducible surface-enhanced Raman scattering substrates based on Ag pyramidal arrays

Yandong Wang¹, Nan Lu¹ (✉), Wentao Wang¹, Lingxiao Liu¹, Lei Feng¹, Zhoufang Zeng¹, Haibo Li¹, Weiqing Xu¹, Zijian Wu², Wei Hu², Yanqing Lu², and Lifeng Chi^{1,3}

¹ State Key Laboratory of Supramolecular Structure and Materials, Jilin University, Changchun 130012, China

² National Laboratory of Solid State Microstructures, Nanjing University, Nanjing 210093, China

³ Physikalisches Institut and Center for Nanotechnology (CeNTech), Westfälische Wilhelms-Universität, D-48149 Münster, Germany

Received: 14 November 2012

Revised: 29 December 2012

Accepted: 2 January 2013

© Tsinghua University Press
and Springer-Verlag Berlin
Heidelberg 2013

KEYWORDS

SERS,
Ag pyramidal array,
reproducibility,
etching,
nanosphere lithography

ABSTRACT

Close-packed Ag pyramidal arrays have been fabricated by using inverted pyramidal pits on Si as a template and used to generate plentiful and homogeneous surface-enhanced Raman scattering (SERS) hot sites. The sharp nanotip and the four edges of the Ag pyramid result in strong electromagnetic field enhancement with an average enhancement factor (EF) of 2.84×10^7 . Moreover, the features of the close-packed Ag pyramidal array can be well controlled, which allows SERS substrates with good reproducibility to be obtained. The relative standard deviation (RSD) was lower than 8.78% both across a single substrate and different batches of substrates.

1 Introduction

Surface-enhanced Raman scattering (SERS) spectroscopy has been intensively explored as a powerful and extremely sensitive analytical technique with applications in biochemistry, chemical production, and environmental monitoring, encouraged by the development of cheaper lasers and spectrometer systems [1, 2]. Since the substrates play a very important

role in SERS measurements, various substrates have been proposed for conducting SERS, which mainly include nanoparticle colloids [3, 4], metallic rough surfaces [5, 6], and periodic nanostructures [7, 8]. The first two categories rely on fundamentally random formations, and have intrinsically limited reproducibility [9]. Although SERS effects with giant enhancement factors (EF) of up to 10^{12} – 10^{13} have been demonstrated for analyte molecules located at so-called

Address correspondence to luenan@jlu.edu.cn

“hot spots”, the fabrication of SERS substrates with a stable, uniform, and high average EF over relatively large areas remains a great challenge [2, 10].

Most of the traditional and commonly-used SERS substrate architectures solely rely on the local electric field enhancement from the small gaps (between two metallic nanostructures) of either roughened metallic surfaces [11–13] or metallic nanoparticles randomly deposited on a surface [14–17]. However, in addition to the small gaps, the sharp corners of the triangular metal nanoparticles prepared by nanosphere lithography also show strong SERS enhancement [18]. Additionally, conical structures with sharp tips have been widely used as highly efficient field emission or field enhancement devices for SERS applications [19, 20].

In general, an ideal SERS substrate should have uniform and plentiful electromagnetic hot sites to enhance the SERS intensities and minimize the deviations [21–25]. So far, few methods have been developed for achieving such kinds of substrates. In this work, we demonstrate a new method to create SERS substrates with plentiful homogeneous hot sites by fabricating Ag pyramidal arrays.

2 Experimental

2.1 Materials

Solvents and chemicals of reagent quality were used without further purification. *N*-octadecyltrimethoxysilane (OTS, 90+% purity) and heptadecafluoro-1,1,2,2-tetrahydrodecyl-triethoxysilane were purchased from Sigma Aldrich. Analytical reagent grade ethanol, acetone, propanol and KOH were purchased from Beijing Chemical Works. The monodisperse polystyrene (PS) spheres with less than 5% diameter variation were also obtained from Sigma Aldrich. One-side polished n-type (100) oriented Si wafers with a resistivity of 0.008–0.02 $\Omega \cdot \text{cm}$ were purchased from GRINM Semiconductor Materials Co. Ltd. Beijing, China.

2.2 Preparation of inverted pyramidal pits

The Si substrates were sonicated in acetone, ethanol, and deionized water for 5 min to remove organic contaminants. The monolayer of PS spheres was prepared as described elsewhere [26, 27]. The substrates

covered with a PS monolayer were heated at 100 °C for 5 min. Then the reactive ion etching (RIE) process was conducted to reduce the size of the PS nanospheres by using a Plasmalab 80 Plus (ICP65) system (Oxford Instruments Co., UK). The etching time for 550 nm spheres was 6 min at a RF power of 30 W, a pressure of 30 mTorr and O₂ flow rate of 20 sccm (standard cubic centimeters per min). Then, an OTS self-assembled monolayer (SAM) was grown on the PS sphere-templated substrate by vapor phase deposition in a vacuum glass desiccator for 6 h at 60 °C. Subsequently, the Si wafers were ultrasonicated in ethanol to remove the PS spheres. A plastic beaker with a magnetic stirrer was used as an etching bath; a hot plate with temperature control probe was used for the bath heating. The chemical etching was carried out by immersing the Si slices in KOH solution under stirring. The size of the pyramidal pits arrays produced was controlled by adjusting the etching duration. Then the sample was rinsed with deionized water to remove KOH.

2.3 Preparation of Ag pyramidal arrays

The fabricated inverted pyramidal Si pits were fluorinated with fluoroalkylsilane (heptadecafluoro-1,1,2,2-tetrahydrodecyl-triethoxysilane) to achieve low surface energy [28]. Then, 400 nm thick silver was thermally evaporated on the fluorinated Si template at a rate of 2.5 nm/min under a pressure of 5×10^{-4} Pa. The Ag layer with pyramidal arrays can be peeled off the wafer surface with sticky tape.

2.4 Characterization

Scanning electron microscope (SEM) images were taken using an environmental scanning electron microscope (ESEM, Model XL 30 ESEM FEG from Micro FEI Philips). The samples were sputtered with a thin layer of Pt (2 nm in thickness) prior to imaging. UV–visible spectra were recorded on a UV–visible spectrometer (Shimadzu UV3600, Shimadzu, Japan). For the SERS detection, the samples were placed in an ethanol solution of benzenethiol for 30 min. Then the samples were rinsed with ethanol for several minutes and dried with nitrogen to remove the unreacted benzenethiol and solvent. An optical fiber portable

Raman spectrometer (B&W Tek Inc.) in backscattering mode was used. The laser line was 532 nm, and the integrating time was varied to avoid over-range. Atomic force microscopy (AFM) was used for the characterization of topography under ambient conditions at room temperature. The AFM instrument (Digital Instruments, Santa Barbara, CA) was operated in tapping mode using silicon nitride cantilevers (Nanosensors, Digital Instruments) with frequencies of 250–350 kHz.

3 Results and discussion

The schematic outline of the fabrication procedure is shown in Fig. 1. First, a monolayer of PS nanospheres was deposited on the Si substrate. Second, the oxygen RIE process was performed to reduce the size of the PS nanospheres according to the application requirement. The 550 nm PS nanospheres were reduced to about 160 nm after etching for 6 min. This process also resulted in the hydroxylation of the Si surface facilitating the growth of the OTS SAM in next step. The OTS SAM was assembled on the PS nanosphere monolayer-masked substrate by vapor phase deposition in a vacuum glass desiccator for 6 h. After organosilane treatment, the Si wafer was ultrasonicated in ethanol to remove the PS nanospheres. The AFM image (Fig. S1 in the Electronic Supplementary Material (ESM)) reveals that an OTS SAM having a periodic pattern with hexagonal geometry at the sub-wavelength scale ($\sim 160 \text{ nm} \pm 5 \text{ nm}$) was formed. The arrangement and density of the pattern were the same as that of original PS sphere monolayer. Next, an inverted

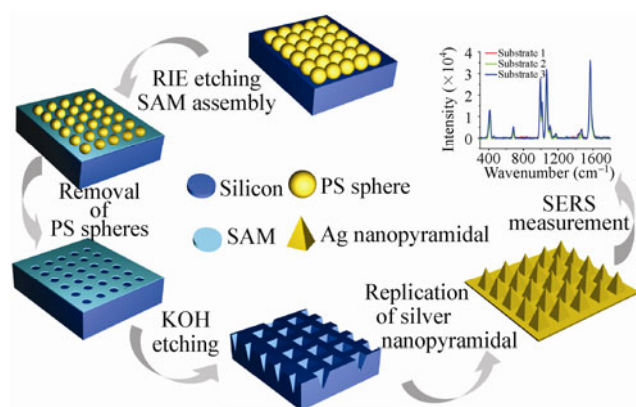


Figure 1 Schematic illustration of the fabrication procedure.

pyramid Si pits array was created by etching the sample with the KOH solution at a certain temperature under stirring. The size of the pyramidal pits was controlled by varying the etching duration. The sample was rinsed with deionized water to remove residual KOH solution. Finally, the Ag pyramidal arrays were created by thermal evaporation utilizing the pyramidal pits array as a template and peeling off with sticky tape.

Figure 2 shows the progression of the inverted pyramidal Si pits array generated with KOH chemical etching. The Si wafers covered with the OTS SAM pattern were etched in a freshly prepared solution of KOH with pH of 11 at 38 °C under stirring. Obviously, the patterns of the masks were accurately transferred onto Si substrate because the periodicity of pyramidal pits is consistent with that of the PS spheres array. The size (basal length) of the pyramidal pits can be controlled by varying the etching duration. The basal lengths were about 160, 186, 214, 266, 315 and 360 nm with etching times of 2, 4, 6, 8, 10 and 12 h, respectively. After etching for 30 min, small pits appeared in the area without the OTS SAM (Fig. S2 in the ESM). The area without the OTS SAM can be selectively etched because its wettability is higher than the area covered by the OTS SAM [29]. The dependence of the basal length of the inverted pyramidal Si pits on the etching time is shown in Fig. S3 in the ESM. It can be observed that the size of the structure created with etching for 2 h ($\sim 160 \text{ nm}$) was approximately the same as the size of the SAM mask ($\sim 160 \text{ nm} \pm 5 \text{ nm}$), and it showed little

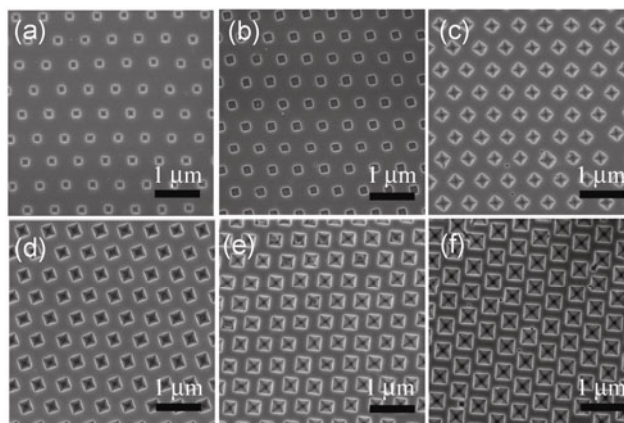


Figure 2 SEM images of the inverted pyramidal Si pits fabricated with different etching times: (a) 2, (b) 4, (c) 6, (d) 8, (e) 10, and (f) 12 h.

iridescence under white light illumination. The etched structure (186 nm) after KOH etching for 4 h also consisted of nanohole arrays without pyramidal pits, as shown in Fig. 2(b). This indicates that the KOH etching reaction started from the blank Si region while its locations were distributed randomly. However, after KOH etching for 6 h, the inverted pyramidal Si pits were quite clearly seen (Fig. 2(c)). With further etching, the basal length of pyramidal pits reached ~360 nm after 12 h (Fig. 2(f)), and they exhibited strong iridescence under white light illumination. The SEM images shown in Figs. 2(c)–2(f) reveal that the sidewalls of pits are very smooth and the anisotropic angle is 54.7° , which is the characteristic KOH etching angle of Si(100). This can be explained in terms of the large difference in the etching rate between the Si<100> and Si<111> surfaces. Due to the different densities of Si atoms on Si<100> and Si<111>, the OH^- etching rate of Si<111> is about 30 times slower than the etching rate of Si<100> [30].

The Ag pyramidal arrays were fabricated by thermal evaporation utilizing the inverted pyramidal Si pits array as a template. The inverted pyramidal Si pits arrays were first fluorinated to reduce the metal adhesion and facilitate peeling of the metal film. Then 400 nm thick Ag was thermally evaporated on the fluorinated Si template at a rate of 2.5 nm/min under a pressure of 5×10^{-4} Pa. The Ag layer with pyramidal array was finally peeled off using sticky tape. Figures 3(a)–3(f) show the tilted-view (45°) SEM images of the Ag pyramidal arrays, which correspond to the inverted pyramidal Si pits templates in Figs. 2(a)–2(f). The basal lengths of the Ag pyramids are about 157, 168, 224, 251, 294 and 348 nm in Figs. 3(a)–3(f), respectively, which mostly match the sizes of the inverted pyramidal Si pit templates. As shown in Figs. 3(a) and 3(b), the replicated Ag arrays exhibit non-pyramidal shape without sharp nanotips, sharp edges or square bases. This is consistent with Figs. 2(a) and 2(b). In contrast, Ag pyramidal arrays with sharp nanotips, sharp edges and square bases were created by using the inverted pyramidal Si pits as templates after etching for 6, 8, 10 and 12 h. It can be observed that the nanotips and four edges of the Ag pyramid became sharper with increasing etching duration. At the same time, the distance between

neighboring Ag pyramids decreased, while the heights of the Ag pyramids increased. The reflection spectra corresponding to the arrays shown in Figs. 3(a)–3(f) are shown in Fig. S4 in the ESM. The sharp nanotips and edges, as well as the decreasing distance between the Ag pyramids should increase the intensities of the SERS signals.

To evaluate the Raman-enhancing capability of the Ag pyramidal arrays, an ethanol solution (10^{-4} M) of benzenethiol was applied to the substrates by dipping the samples in benzenethiol solution for 30 min. In Fig. 4, the Raman spectra from bottom to top correspond to the samples presented in Figs. 3(a)–3(f). The peaks observed for the different sized Ag pyramidal arrays can be assigned according to the literature [31–34]. The peak at $1,469\text{ cm}^{-1}$ is evidence of the formation of Ag–S bonds. The peak at $1,570\text{ cm}^{-1}$ comes from the C–C stretching, whereas the peaks at $1,066\text{ cm}^{-1}$, $1,017\text{ cm}^{-1}$ and 996 cm^{-1} can be assigned to the in-plane phenyl ring stretching band, the in-plane ring deformation, and the in-plane ring deformation mode coupled to the S–H bending mode, respectively. The peaks at 684 cm^{-1} and 413 cm^{-1} are ascribed to the C–H out-of-plane deformation and C–S stretching. The absence of a peak at 917 cm^{-1} indicates that benzenethiol was chemisorbed onto Ag by rupturing the S–H bond, while the presence of both in-plane and out-of-plane vibration modes indicates that the chemisorbed benzenethiol has a tilted orientation on the Ag surface. The Raman intensities increase significantly when the Ag pyramidal arrays have

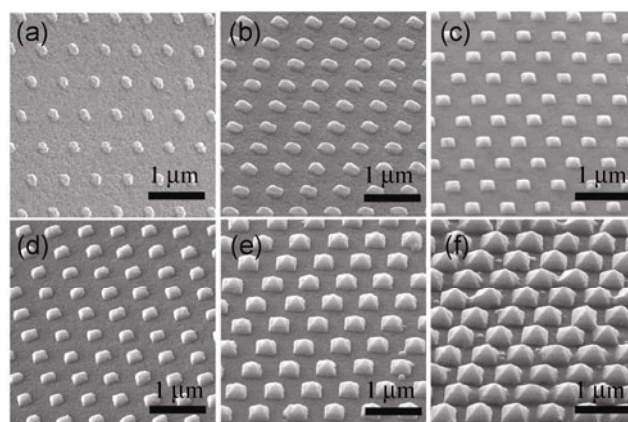


Figure 3 Tilted-view (45°) SEM images of the Ag pyramidal arrays replicated from the Si templates (templates (a)–(f) in Fig. 2).

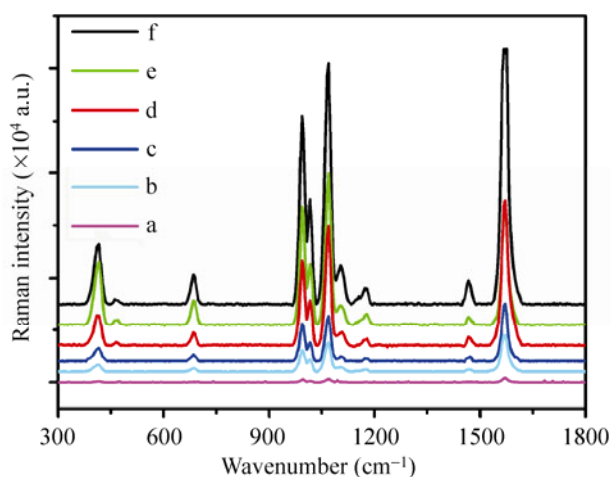


Figure 4 SERS spectral comparison of 10^{-4} M benzenethiol adsorbed on the Ag pyramidal arrays with different sizes (samples (a)–(f) in Fig. 3). The integration time is 1 s.

sharp nanotips and sharp edges, and when the distance between the neighboring Ag pyramids is reduced. Therefore, in order to obtain close-packed Ag pyramidal arrays with sharp nanotips and sharp edges, the corresponding reverse close-packed Si inverted pyramidal pits array should be fabricated.

As shown in Fig. 5(a), such inverted pyramidal Si pit arrays were formed after KOH etching (pH = 13) for 10 min at 50 °C, in which the inverted pyramidal pits are in a close-packed arrangement, similar to the PS monolayer. The etching duration was reduced by increasing the concentration and temperature of the KOH solution. The magnified SEM image shown as an inset in Fig. 5(a) reveals that the surface on the top is rougher due to the vigorous KOH etching, which may also result in stronger Raman intensities. The close-packed Ag pyramidal arrays are shown in Fig. 5(b). The stem diameter is around 520 nm, and the radius of curvature of Ag pyramids is less than 5 nm [35]. The UV–visible spectrum and simulation of the close-packed Ag pyramids are shown in Fig. 5(c). The main absorption peaks are observed at ~527 and ~624 nm, and should originate from the periodic hexagonal close-packing arrangement. The result is consistent with the spectrum simulated by the rigorous coupled-wave analysis (RCWA) method. To study the electromagnetic field distribution in the Ag pyramidal array, a 3D finite-difference time-domain (FDTD) simulation was carried out using a commercial

software package (Lumerical FDTD Solution 7.1, Inc., Canada). The model and simulation results are shown in Fig. 5(d), where the basal length and the period of the Ag pyramids is 520 nm and 550 nm, respectively. The grid was set as a 6.0 nm cube in the calculations. The Ag dielectric constant is from Johnson and Christy [36]. A periodic boundary condition was used in the simulation because the array is ordered. A 532 nm sinusoidal plane electromagnetic wave with normal incident was chosen in the simulations. The calculations indicate that localized plasmons and substantial electromagnetic field enhancement are generated on the nanotips and the edges/sides. It has been reported that a very small percentage of molecules (0.0063%) in the hottest spots contribute 24% to the overall SERS intensity [37], and thus the close-packed Ag pyramidal array should give stronger intensities in SERS measurements. To evaluate the enhancement ability of the close-packed Ag pyramidal array, the enhancement factor (EF) was calculated by comparing the signal intensities in SERS and normal Raman spectra. According to a previous report [38], the EF can be calculated following the formula $EF = (I_{\text{SERS}}/I_{\text{REF}}) \times (N_{\text{REF}}/N_{\text{SERS}})$, where N_{SERS} and N_{REF} are the numbers of benzenethiol molecules contributing to the SERS signal and the normal Raman signal, respectively, and I_{SERS} and I_{REF} are the intensities of the selected

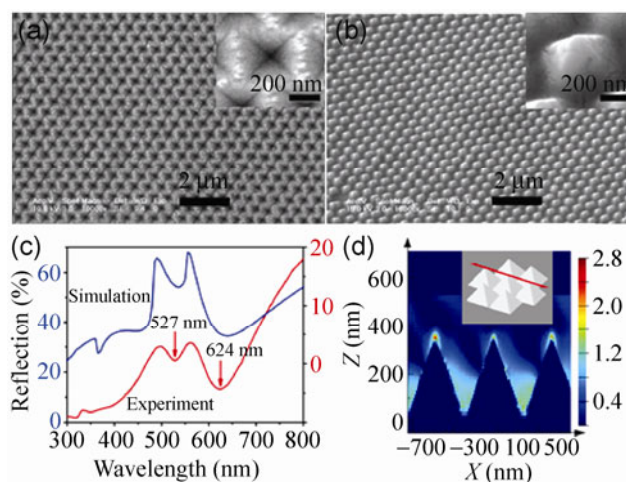


Figure 5 SEM images of the close-packed inverted pyramidal Si pits (a) and Ag pyramidal array (b); the inset images in (a) and (b) are the corresponding magnified SEM images. The measured and simulated reflection spectra (c) and the 3D-FDTD simulation (d) of the close-packed Ag pyramidal array.

scattering bands in the SERS and normal Raman spectra, respectively. Figure 6 shows the SERS spectra of benzenethiol molecules with concentration of 10^{-6} and 10^{-8} M adsorbed on the Ag pyramidal arrays, and the normal Raman spectra of benzenethiol aqueous solution (10 M, 10 μ L) on the blank Si substrate and 10^{-2} M (10 μ L) ethanol solution on the flat Ag substrate. Evident Raman signals with little background noise are obtained on the Ag pyramidal array with concentrations of 10^{-8} M and above. Without SERS originating from Ag pyramids, no distinguishable peak was observed for 1 mM benzenethiol on the flat Ag substrate (data not shown) and relatively weak peaks were found for 10 mM benzenethiol on the flat Ag substrate. According to the Ref. [39], the molecular packing density for benzenethiol on Ag is 0.554 nmol/cm^2 , assuming that benzenethiol is adsorbed on the substrate as a homogeneous monolayer, and the average area occupied by each benzenethiol molecule is estimated to be 30.6 nm^2 . The effective focused depth and the diameter of the laser spot are 21 μm and 1 μm respectively according to the optical configuration and the microscope with a 514.5 nm laser. N_{SERS} is calculated to be 0.257×10^5 . The reference used for non-SERS measurements is 10 M benzenethiol

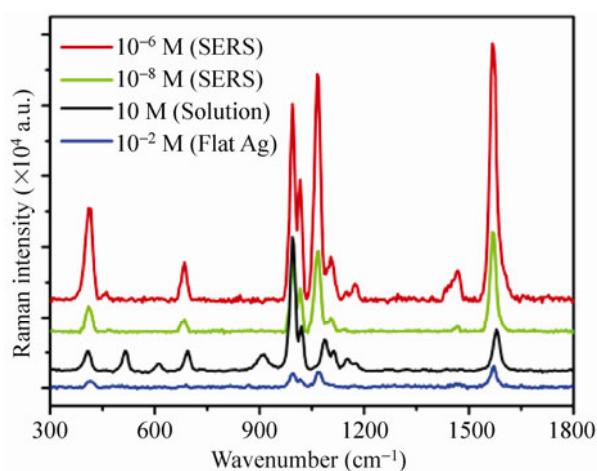


Figure 6 SERS spectra of benzenethiol molecules with concentration of 10^{-6} and 10^{-8} M adsorbed on the Ag pyramidal arrays, the normal Raman spectra of benzenethiol aqueous solution (10 M, 10 μ L) on the blank Si substrate and 10^{-2} M (10 μ L) ethanol solution on the flat Ag substrate, respectively. The integration time is 5 s for the SERS and solution measurements, and 30 s for the flat Ag substrate.

aqueous solution, contributing about 1.0×10^{11} benzenethiol molecules. Based on the intensities of peaks at 1,570, 1,066 and 413 cm^{-1} , the average EF factors are 2.48×10^7 , 2.84×10^7 and 1.90×10^7 respectively. These results should be attributed to the large electromagnetic field enhancement on the sharp nanotip and the four sharp edges, as well as the surface plasma progression on the Ag pyramidal array (consisting of the Ag pyramids and the underlying Ag layer).

A good SERS substrate exhibits not only high enhancement ability but also good reproducibility. To evaluate the reproducibility of the Ag pyramidal arrays, the three Ag pyramidal arrays shown in Fig. 5 were fabricated with the same Si template successively. The SERS spectra of benzenethiol molecules with a concentration of 10^{-6} M on these three Ag pyramidal arrays are shown in Figs. 7(a)–7(c). To investigate the homogeneity of each substrate, SERS spectra were collected on 20 randomly selected points on each substrate. The results indicate that the Ag pyramidal arrays possess excellent homogeneity in SERS performance. In order to examine the reproducibility of the three different batches in SERS measurements, a comparison of the SERS spectra is shown in Fig. 7(d). It can be observed that the reproducibility of the

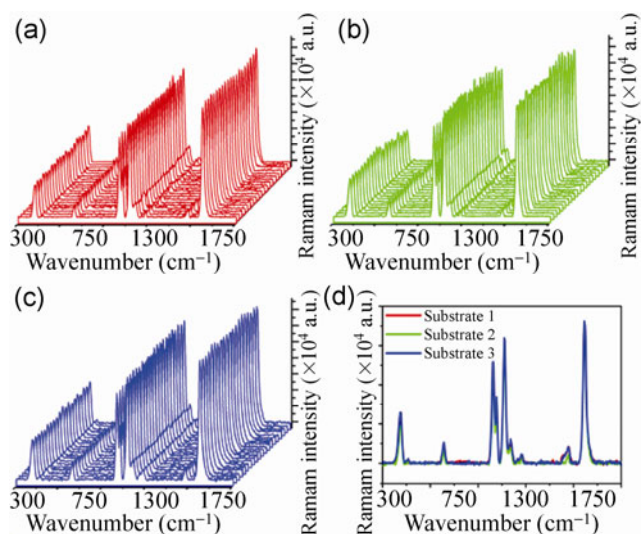


Figure 7 SERS spectra of benzenethiol molecules with a concentration of 10^{-6} M adsorbed on three different batches ((a)–(c)) of Ag pyramidal arrays at 20 randomly selected points. Panel d shows the SERS spectra from these Ag pyramidal arrays. The integration time is 5 s.

different batches of Ag pyramidal arrays is good. To further investigate the reproducibility of the Ag pyramidal arrays, three peaks at 413, 996 and 1,570 cm^{-1} were chosen to calculate the relative standard deviation (RSD) of Raman intensities from spot-to-spot, and sample-to-sample, and the results are shown in detail in Table S1 in the ESM. The values of RSD for all the samples are lower than 8.78%, which confirms that the reproducibility is good.

4 Conclusions

A new method for fabricating highly effective and reproducible SERS substrates has been demonstrated. With this method, Ag pyramidal arrays were created and used for SERS measurements. The close-packed Ag pyramidal arrays exhibit excellent Raman enhancement performance with an EF value of 2.84×10^7 . A 3D-FDTD simulation reveals that the Ag pyramid produces a large electromagnetic field enhancement around the nanotip and the four edges/sides. Moreover, the Ag pyramidal array can be created consistently, eliminating structural variations caused by the process fluctuations existing in other fabrication techniques. The close-packed Ag pyramidal array exhibits excellent homogeneity and reproducibility with RSDs lower than 8.78% across one substrate and different batches of substrates, respectively. This makes the method an ideal candidate for fabricating inexpensive and reproducible SERS substrates.

Acknowledgements

This work was supported by the National Natural Science Foundation of China (Nos. 21273092 and 20373019) and the National Basic Research Program (No. 2009CB939701).

Electronic Supplementary Material: An AFM image of the OTS SAM on Si substrate, SEM image of the pits after chemical etching for 30 min, dependence of the size (basal length) of the inverted pyramidal Si pits on the etching time, the reflection spectra corresponding to the arrays shown in Figs. 3(a)–3(f) and the RSD values of the peaks (at 413, 996, and 1,570 cm^{-1}) from the three different batches of Ag

pyramidal arrays, are available in the online version of this article at <http://dx.doi.org/10.1007/s12274-013-0291-0>.

References

- [1] Schierhorn, M.; Lee, S. J.; Boettcher, S. W.; Stucky, G. D.; Moskovits, M. Metal–silica hybrid nanostructures for surface-enhanced Raman spectroscopy. *Adv. Mater.* **2006**, *18*, 2829–2832.
- [2] Fang, J.; Du, S.; Lebedkin, S.; Li, Z.; Kruk, R.; Kappes, M.; Hahn, H. Gold mesostructures with tailored surface topography and their self-assembly arrays for surface-enhanced Raman spectroscopy. *Nano Lett.* **2010**, *10*, 5006–5013.
- [3] Haynes, C. L.; McFarland, A. D.; Van Duyne, R. P. Surface-enhanced Raman spectroscopy. *Anal. Chem.* **2005**, *77*, 338A–346A.
- [4] Lee, S. J.; Guan, Z.; Xu, H.; Moskovits, M. Surface-enhanced Raman spectroscopy and nanogeometry: The plasmonic origin of SERS. *J. Phys. Chem. C* **2007**, *111*, 17985–17988.
- [5] Oh, Y. J.; Jeong, K. H. Glass nanopillar arrays with nanogap-rich silver nanoislands for highly intense surface enhanced Raman scattering. *Adv. Mater.* **2012**, *24*, 2234–2237.
- [6] Lu, G.; Li, H.; Wu, S.; Chen, P.; Zhang, H. High-density metallic nanogaps fabricated on solid substrates used for surface enhanced Raman scattering. *Nanoscale* **2012**, *4*, 860–863.
- [7] Mu, C.; Zhang, J. P.; Xu, D. Au nanoparticle arrays with tunable particle gaps by template-assisted electroless deposition for high performance surface-enhanced Raman scattering. *Nanotechnology* **2010**, *21*, 015604.
- [8] Wang, Y.; Becker, M.; Wang, L.; Liu, J.; Scholz, R.; Peng, J.; Goesele, U.; Christiansen, S.; Kim, D. H.; Steinhart, M. Nanostructured gold films for SERS by block copolymer-templated galvanic displacement reactions. *Nano Lett.* **2009**, *9*, 2384–2389.
- [9] Kostovski, G.; White, D. J.; Mitchell, A.; Austin, M. W.; Stoddart, P. R. Nanoimprinted optical fibres: Biotemplated nanostructures for SERS sensing. *Biosens. Bioelectron.* **2009**, *24*, 1531–1535.
- [10] Li, J. F.; Huang, Y. F.; Ding, Y.; Yang, Z. L.; Li, S. B.; Zhou, X. S.; Fan, F. R.; Zhang, W.; Zhou, Z. Y.; Wu, D. Y.; Ren, B.; Wang, Z. L.; Tian, Z. Q. Shell-isolated nanoparticle-enhanced Raman spectroscopy. *Nature* **2010**, *464*, 392–395.
- [11] Fleischmann, M.; Hendra, P. J.; McQuillan, A. J. Raman-spectra of pyridine adsorbed at a silver electrode. *Chem. Phys. Lett.* **1974**, *26*, 163–166.
- [12] Sajanlal, P. R.; Pradeep, T. Mesoflowers: A new class of highly efficient surface-enhanced Raman active and infrared-absorbing materials. *Nano Res.* **2009**, *2*, 306–320.

- [13] Albrecht, M. G.; Creighton, J. A. Anomalous intense Raman-spectra of pyridine at a silver electrode. *J. Am. Chem. Soc.* **1977**, *99*, 5215–5217.
- [14] Kerker, M.; Wang, D. S.; Chew, H. Surface enhanced Raman scattering (SERS) by molecules adsorbed at spherical particles: Errata. *Appl. Opt.* **1980**, *19*, 4159–4174.
- [15] Panigrahi, S.; Prahara, S.; Basu, S.; Ghosh, S. K.; Jana, S.; Pande, S.; Vo-Dinh, T.; Jiang, H.; Pal, T. Self-assembly of silver nanoparticles: Synthesis, stabilization, optical properties, and application in surface-enhanced Raman scattering. *J. Phys. Chem. B* **2006**, *110*, 13436–13444.
- [16] Braun, G.; Lee, S. J.; Dante, M.; Nguyen, T. Q.; Moskovits, M.; Reich, N. Surface-enhanced Raman spectroscopy for DNA detection by nanoparticle assembly onto smooth metal films. *J. Am. Chem. Soc.* **2007**, *129*, 6378–6379.
- [17] Tao, A.; Kim, F.; Hess, C.; Goldberger, J.; He, R. R.; Sun, Y. G.; Xia, Y. N.; Yang, P. D. Langmuir–Blodgett silver nanowire monolayers for molecular sensing using surface-enhanced Raman spectroscopy. *Nano Lett.* **2003**, *3*, 1229–1233.
- [18] Stiles, P.; Dieringer, J.; Shah, N. C.; Van Duyne, R. P. Surface-enhanced Raman spectroscopy. *Annu. Rev. Anal. Chem.* **2008**, *1*, 601–626.
- [19] Wu, W.; Hu, M.; Ou, F. S.; Li, Z.; Williams, R. S. Cones fabricated by 3D nanoimprint lithography for highly sensitive surface enhanced Raman spectroscopy. *Nanotechnology* **2010**, *21*, 255502.
- [20] Yang, Y.; Li, Z. Y.; Yamaguchi, K.; Tanemura, M.; Huang, Z.; Jiang, D.; Chen, Y.; Zhou, F.; Nogami, M. Controlled fabrication of silver nanoneedles array for SERS and their application in rapid detection of narcotics. *Nanoscale* **2012**, *4*, 2663–2669.
- [21] Lin, X. M.; Cui, Y.; Xu, Y. H.; Ren, B.; Tian, Z. Q. Surface-enhanced Raman spectroscopy: Substrate-related issues. *Anal. Bioanal. Chem.* **2009**, *394*, 1729–1745.
- [22] Schierhorn, M.; Lee, S. J.; Boettcher, S. W.; Stucky, G. D.; Moskovits, M. Metal-silica hybrid nanostructures for surface-enhanced Raman spectroscopy. *Adv. Mater.* **2006**, *18*, 2829–2832.
- [23] Li, X.; Hu, H.; Li, D.; Shen, Z.; Xiong, Q.; Li, S.; Fan, H. J. Ordered array of gold semishells on TiO₂ spheres: An ultrasensitive and recyclable SERS substrate. *ACS Appl. Mater. Interf.* **2012**, *4*, 2180–2185.
- [24] Krishnamoorthy, S.; Krishnan, S.; Thoniyot, P.; Low, H. Y. Inherently reproducible fabrication of plasmonic nanoparticle arrays for SERS by combining nanoimprint and copolymer lithography. *ACS Appl. Mater. Interf.* **2011**, *3*, 1033–1040.
- [25] Qian, L.; Mookherjee, R. Convective assembly of linear gold nanoparticle arrays at the micron scale for surface enhanced Raman scattering. *Nano Res.* **2011**, *4*, 1117–1128.
- [26] Xu, H. B.; Lu, N.; Qi, D. P.; Hao, J. Y.; Gao, L. G.; Zhang, B.; Chi, L. F. Biomimetic antireflective Si nanopillar arrays. *Small* **2008**, *4*, 1972–1975.
- [27] Wang, Y. D.; Lu, N.; Xu, H. B.; Shi, G.; Xu, M. J.; Lin, X. W.; Li, H. B.; Wang, W. T.; Qi, D. P.; Lu, Y. Q.; Chi, L. F. Biomimetic corrugated silicon nanocone arrays for self-cleaning antireflection coatings. *Nano Res.* **2010**, *3*, 520–527.
- [28] Zeng, Z. F.; Wang, Y. D.; Shi, S. L.; Wang, L. F.; Guo, X. H.; Lu, N. On-plate selective enrichment and self-desalting of peptides/proteins for direct MALDI MS analysis. *Anal. Chem.* **2012**, *84*, 2118–2123.
- [29] Wang, W. T.; Lu, N.; Hao, J. Y.; Xu, H. B.; Qi, D. P.; Chi, L. F. Self-assembled monolayer islands masked chemical etching for broadband antireflective silicon surfaces. *J. Phys. Chem. C* **2010**, *114*, 1989–1995.
- [30] Seidel, H.; Csepregi, L.; Heuberger, A.; Baumgartel, H. Anisotropic etching of crystalline silicon in alkaline solutions. *J. Electrochem. Soc.* **1990**, *137*, 3612–3626.
- [31] Jung, H. Y.; Park, Y. K.; Park, S.; Kim, S. K. Surface enhanced Raman scattering from layered assemblies of close-packed gold nanoparticles. *Anal. Chim. Acta* **2007**, *602*, 236–243.
- [32] Mahmoud, M. A.; El-Sayed, M. A. Aggregation of gold nanoframes reduces, rather than enhances, SERS efficiency due to the trade-off of the inter- and intraparticle plasmonic fields. *Nano Lett.* **2009**, *9*, 3025–3031.
- [33] Biggs, K. B.; Camden, J. P.; Anker, J. N.; Van Duyne, R. P. Surface-enhanced Raman spectroscopy of benzenethiol adsorbed from the gas phase onto silver film over nanosphere surfaces: Determination of the sticking probability and detection limit time. *J. Phys. Chem. A* **2009**, *113*, 4581–4586.
- [34] McFarland, A. D.; Young, M. A.; Dieringer, J. A.; Van Duyne, R. P. Wavelength-scanned surface-enhanced Raman excitation spectroscopy. *J. Phys. Chem. B* **2005**, *109*, 11279–11285.
- [35] Linn, N. C.; Sun, C. H.; Arya, A.; Jiang, P.; Jiang, B. Surface-enhanced Raman scattering on periodic metal nanotips with tunable sharpness. *Nanotechnology* **2009**, *20*, 225303.
- [36] Johnson, P. B.; Christy, R. W. Optical constants of the noble metals. *Phys. Rev. B* **1972**, *6*, 4370–4379.
- [37] Fang, Y.; Seong, N. H.; Dlott, D. D. Measurement of the distribution of site enhancements in surface-enhanced Raman scattering. *Science* **2008**, *321*, 388–392.
- [38] Ji, N.; Ruan, W.; Wang, C.; Lu, Z.; Zhao, B. Fabrication of silver decorated anodic aluminum oxide substrate and its optical properties on surface-enhanced Raman scattering and thin film interference. *Langmuir* **2009**, *25*, 11869–11873.
- [39] Gui, J.; Stern, D.; Frank, D.; Lu, F.; Zapien, D.; Hubbard, A. Adsorption and surface structural chemistry of thiophenol, benzyl mercaptan, and alkyl mercaptans. Comparative studies at Ag(111) and Pt(111) electrodes by means of Auger spectroscopy, electron energy loss spectroscopy, low-energy electron diffraction, and electrochemistry. *Langmuir* **1991**, *7*, 955–963.